Genomics

Molecular Cancer Research

Genomic cfDNA Analysis of Aqueous Humor in Retinoblastoma Predicts Eye Salvage: The Surrogate Tumor Biopsy for Retinoblastoma

Jesse L. Berry[1,2], Liya Xu[3], Irsan Kooi[4], A. Linn Murphree[1,2], Rishvanth K. Prabakar[5], Mark Reid[1], Kevin Stachelek[1], Bao Han A. Le[1,2], Lisa Welter[3], Bibiana J. Reiser[1,2], Patricia Chévez-Barrios[6], Rima Jubran[7], Thomas C. Lee[1,2], Jonathan W. Kim[1,2], Peter Kuhn[3,8,9,10], David Cobrinik[1,2,8,11,12], and James Hicks[3,8]

Abstract

Tumor-derived cell-free DNA (cfDNA) has biomarker potential; therefore, this study aimed to identify cfDNA in the aqueous humor (AH) of retinoblastoma eyes and correlate somatic chromosomal copy-number alterations (SCNA) with clinical outcomes, specifically eye salvage. AH was extracted via paracentesis during intravitreal injection of chemotherapy or enucleation. Shallow whole-genome sequencing was performed using isolated cfDNA to assess for highly recurrent SCNAs in retinoblastoma including gain of 1q, 2p, 6p, loss of 13q, 16q, and focal *MYCN* amplification. Sixty-three clinical specimens of AH from 29 eyes of 26 patients were evaluated; 13 eyes were enucleated and 16 were salvaged (e.g., saved). The presence of detectable SCNAs was 92% in enucleated eyes versus 38% in salvaged eyes ($P = 0.006$). Gain of chromosome 6p was the most common SCNA found in 77% of enucleated eyes, compared with 25% of salvaged eyes ($P = 0.0092$), and associated with a 10-fold increased odds of enucleation (OR, 10; 95% CI, 1.8–55.6). The median amplitude of 6p gain was 1.47 in enucleated versus 1.07 in salvaged eyes ($P = 0.001$). The presence of AH SCNAs was correlated retrospectively with eye salvage. The probability of ocular salvage was higher in eyes without detectable SCNAs in the AH ($P = 0.0028$), specifically 6p gain. This is the first study to correlate clinical outcomes with SCNAs in the AH from retinoblastoma eyes, as such these findings indicate that 6p gain in the aqueous humor is a potential prognostic biomarker for poor clinical response to therapy.

Implications: The correlation of clinical outcomes and SCNAs in the AH identified in the current study requires prospective studies to validate these finding before SCNAs, like 6p gain, can be used to predict clinical outcomes at diagnosis. *Mol Cancer Res; 16(11); 1701–12. ©2018 AACR.*

Introduction

Retinoblastoma is a primary cancer that develops in the eyes of children. Although various treatment modalities exist, enucleation, or surgical removal of the entire eye, is still needed for advanced tumors (1, 2). Primary enucleation is performed when the tumor appears to be too advanced for attempted salvage therapy. Secondary enucleation is required when the tumor recurs after chemotherapy and the eye is removed to prevent tumor spread. Currently, prediction of which eyes will respond to therapy (and avoid enucleation) is based on clinical classifications, which include tumor size, retinal detachment, and tumor seeding (3). However, the most commonly used classification, the International Intraocular Retinoblastoma Classification (IIRC; ref. 3), is predictive of treatment success in only 50% of group D eyes (4, 5) and is even less predictive for more advanced group E eyes (6, 7). A better method for predicting eye salvage and response to therapy is critically needed for retinoblastoma patients.

A notable difference in the classification of retinoblastoma compared with other cancers is that it is not based on biopsy

[1]The Vision Center at Children's Hospital Los Angeles, Los Angeles, California. [2]USC Roski Eye Institute, Keck Medical School of the University of Southern CA, Los Angeles, California. [3]Department of Biological Sciences, Dornsife College of Letters, Arts, and Sciences, University of Southern California, Los Angeles, California. [4]Leiden, the Netherlands. [5]Department of Molecular and Computational Biology, University of Southern California, Los Angeles, California. [6]Departments of Pathology and Genomic Medicine and Ophthalmology, Houston Methodist, Weill Cornell Medical College, Houston, Texas. [7]The Children's Center for Cancer and Blood Diseases, Children's Hospital Los Angeles, Los Angeles, California. [8]Norris Comprehensive Cancer Center, Keck School of Medicine, University of Southern California, Los Angeles, California. [9]Department of Aerospace and Mechanical Engineering, Viterbi School of Engineering, University of Southern California, Los Angeles, California. [10]Department of Biomedical Engineering, Viterbi School of Engineering, University of Southern California, Los Angeles, California. [11]Department of Biochemistry and Molecular Medicine, Keck School of Medicine, University of Southern California, Los Angeles, California. [12]The Saban Research Institute, Children's Hospital Los Angeles, Los Angeles, California.

Note: Supplementary data for this article are available at Molecular Cancer Research Online (http://mcr.aacrjournals.org/).

Prior presentations: European Ocular Oncology Group, March 2018; Association for Research in Vision and Ophthalmology, May 2018; American Society of Clinical Oncology, June 2018; Liquid Biopsy Summit, June 2018; Association for Research in Vision and Ophthalmology Oncogenesis, July 2018.

Corresponding Author: Jesse L. Berry, Children's Hospital Los Angeles and the USC Roski Eye Institute, 4650 Sunset Blvd MS#88, Los Angeles, CA 90027. Phone: 323-442-6335; E-mail: jesse.berry@med.usc.edu

doi: 10.1158/1541-7786.MCR-18-0369

and does not consider any genetic tumor markers (8). Nonetheless, much is known about retinoblastoma genetics from studies of tumors in enucleated eyes. The vast majority of retinoblastoma (98%) is initiated by inactivation of both alleles of the *RB1* tumor suppressor gene on chromosome 13q (9–13). Additional genetic changes can further drive tumorigenesis (14, 15). Tumor studies have revealed somatic copy-number alteration (SCNA) profiles with highly recurrent chromosomal gains on 1q, 2p, 6p, losses on 13q, 16q, and focal *MYCN* amplification on 2p, which together are termed "RB SCNAs" (9, 10, 12, 13).

The role RB SCNAs play in retinoblastoma tumorigenesis and, moreover, whether there are certain SCNAs that portend a more aggressive tumor phenotype is unknown. One report suggests that 1q and 6p gain and 16q loss may be associated with locally invasive disease (16); another suggests that gain of 6p is associated with less differentiated tumors with higher rates of optic nerve invasion (17), and may be seen in older patients (18). However, these associations have not been relevant to predicting eye salvage nor applied to tumors at diagnosis or during therapy. This is because invasive tissue biopsy of retinoblastoma is contraindicated for fear of extraocular tumor spread (19, 20).

To overcome the problem of inability to biopsy, we recently demonstrated that tumor-derived cell-free DNA (cfDNA) is present in the aqueous humor (AH; ref. 21), which can be safely extracted from retinoblastoma eyes undergoing therapy (22). Thus, the goals of this study were to determine whether genomic analysis of the AH samples reproducibly reflects the genomic state of the tumor and whether the highly recurrent RB SCNAs detected in the AH predict tumor response to therapy and thus the ability to salvage the eye.

Materials and Methods

Institutional Review Board approval was obtained with written informed consent from the parents of participants. Samples were sequenced within 1 month of extraction.

Patient selection

This analysis included patients diagnosed with retinoblastoma from December 2014 to August 2017 who underwent intravitreal injection of melphalan (IVM) during routine clinical therapy or underwent enucleation (either as primary or secondary), and for whom AH samples were taken and parental consent was obtained. No patients meeting these criteria were excluded. Therapy was not randomized but done per CHLA protocol (5, 23). The primary endpoint was eye salvage (e.g., the ability to treat the cancer and save the eye with standard clinical therapy).

Control samples include 0.1 mL of AH from 2 patients with congenital glaucoma and one with pediatric cataract. None were infectious or inflammatory in etiology.

Genomic data were kept separate from the clinical data until final analysis, which was done retrospectively. REMARK guidelines for reporting biomarkers were followed (24).

Surgical procedure and specimen storage

Clear corneal paracentesis was performed with extraction of 0.1 mL of AH as part of the procedure for intravitreal injection of chemotherapy (25) or immediately after enucleation. After intravitreal injection of chemotherapy, cryotherapy is applied to the scleral injection site. Cryotherapy is not done at the corneal paracentesis site.

For control patients, corneal paracentesis was done as part of routine anterior segment surgery.

Samples were stored at −80°C without other preservation. CfDNA isolation and sequencing protocols were described previously (21).

Data analysis

DNA concentrations were assayed using Qubit HS (High-Sensitivity) kits (Thermo Fisher). SCNA analyses were described previously (21, 26, 27). Next-generation sequencing reads from pooled barcoded DNA libraries were deconvoluted (Illumina iGenome) and mapped to the human genome (hg19, Genome Reference Consortium GRCh37; ref. 28) with Bowtie2 (29, 30). Duplicates were removed (samtools rmdup; ref. 31), normalized for G:C content, and DNA segment copy numbers were obtained by dividing the genome into 5,000 variable length bins and calculating the relative number of reads in each bin. Copy-number estimates were calculated by reference-free log2 ratios taking the median window count of normal autosomal chromosomes. Segmentation was performed using circular binary segmentation with DNAcopy (Bioconductor; ref. 32). SCNAs were positive at 20% deflection from baseline (log2 ratio = 0), meaning losses at log2 ratios <−0.2 (ratio of 0.87 or lower) and gains at log2 ratios >0.2 (ratio of 1.15 or higher). Hierarchical clustering was performed using heatmap.2 function in R package gplots ((https://cran.r-project.org/web/packages/gplots/index.html) on median-centered data, using Ward method (33, 34) as the distance metric. Clustering was based on the Pearson correlation of the SCNA profiles. When tumor was available, concordance was determined by dividing the median-segmented ratio values for the tumor by the median-segmented ratio values for the AH and calculating the percentage of bins in which the ratio was within 0.8 to 1.2 (excluding chromosomes X and Y; ref. 35).

Genomic instability was calculated as the sum of the segmented log2 ratios, excluding chromosomes X and Y and represented as the sum deviation from the median. AH samples with <2% of reads aligned to the human genome were removed from analysis.

Fisher exact tests were used for associations between presence of RB SCNAs and clinical classification, or outcome. Kaplan–Meier survival analyses with log-rank tests compared eye salvage in treated eyes based on IIRC groups (3) and presence of any RB SCNAs, as well as each SCNA individually (modeled as presence/absence given at least 20% deflection from baseline).

A Cox proportional hazard model was used to assess the viability of genomic instability as a biomarker. The method was also used to estimate hazard ratios of all candidate RB SCNAs, while accounting for patient age and staging. Because of low frequency of SCNAs other than 6p, we created another proportional hazard model that considered the interaction between 6p and any other candidate SCNA, while accounting for age, to estimate hazard of enucleation. To validate this multivariable model and avoid estimation bias, we utilized bootstrapping with 500 replications. A mixed-model test compared median amplitudes of 6p gain in enucleated versus salvaged eyes, accounting for biological replicates and within-patient variations by eye. JMP Pro 13 (SAS Institute, Inc.) and Stata/SE 14.2 (StataCorp) were used for statistical analyses. Because of the small sample size inherent in studies of pediatric retinoblastoma, we did not conduct any internal validation by split-sample or cross-validation. We did conduct bootstrapping on a limited Cox hazard model considering 6p gain and its interaction with other RB SCNAs (1q, 2p, and 16q).

Charts were reviewed for age at diagnosis, sex, laterality, IIRC group (3), treatment modalities, tumor recurrence, enucleation, and follow-up.

Results

Patients and samples

To assess relationships between retinoblastoma AH SCNAs and clinical features, we assembled a data set including sequential AH samples, matched tumors from enucleated eyes and clinical outcomes. Demographics of the 26 patients are presented in Table 1; 3 patients had both eyes included for a total of 29 eyes. Thirteen eyes required enucleation (3 primarily and 10 secondarily due to tumor relapse). Sixteen eyes were salvaged with treatment. Treatment was not randomized and included 3-drug intravenous chemotherapy (CEV; refs. 5, 23), intra-arterial chemotherapy, intravitreal chemotherapy for seeding (IVM; refs. 36, 37) during which AH samples were taken, and consolidation with laser and cryotherapy. The number of laser and cryotherapy sessions are listed in Table 1 and did not vary between enucleated and salvaged eyes ($P = 0.92$). Clinical follow-up from diagnosis to last evaluation ranged from 8 to 49 months (median, 19 months). No eye that was considered salvaged had less than 12 months of follow-up. All eyes evaluated in this study were advanced, with seeding, which may present a selection bias; however, the presence of RB SCNAs did not correlate with seed class (ref. 38; $P = 0.12$). The median age at diagnosis did not differ significantly between enucleated and salvaged eyes (enucleated median 20 months, range 0 to 38 months; salvaged median age 10 months, range 2 to 59 months, $P = 0.66$). For all patients, peripheral blood cells were tested for *RB1* mutations and the results are shown in Table 1.

CfDNA concentration was measured for 8 eyes (18 samples) and ranged from 0.084 to 56 nanograms/microliter (ng/μL). The DNA concentrations are listed in Table 1, by eye. If more than 1 AH sample was evaluated per eye, a median value was given. The AH median concentration of cfDNA obtained at the time of melphalan treatment was 0.2 ng/μL. As described previously (21), eyes with large untreated tumors that underwent primary enucleation had much higher concentrations (mean, 43.6 ng/μL). Excluding the primarily enucleated eyes (which were also excluded from survival analysis), there was no difference in the concentration of cfDNA from eyes that were salvaged versus those that were enucleated ($P = 0.19$). CfDNA concentration was not measured for every AH sample. For the control samples of AH, median concentration of DNA in the AH was found to be 0.15 ng/μL (mean, 0.12; range, 0.05–0.16 ng/μL).

Tumor tissue was taken and available for comparison with AH of the 13 enucleated eyes. Histopathologic analysis of enucleated eyes revealed active tumor with mitosis and apoptosis; vitreous seeds were documented on histopathology from all enucleated eyes. No tumor was seen in the needle tracks from the paracentesis site in the cornea or from the scleral needle tracks for injection of melphalan into the vitreous (Fig. 1). The cornea tracks were well healed and without tumor (Fig. 1A–C). The pars plana entrance of the injection site also showed healed tissue without tumor cells (Fig. 1D and E). These findings are consistent with the lack of tumor cells in each of 10 AH samples previously examined (21) and indicate that tumor-DNA copy-number alteration (CNA) profiles derive from cfDNA that has perfused into the anterior chamber.

Spectrum of genomic changes in AH cfDNA

We obtained genome-wide SCNA profiles from AH cfDNA by shallow whole-genome sequencing, followed by assigning mapped reads to preassigned "bins" across the genome (26, 39). Thirteen tumor and 63 AH samples were included; 5 obtained immediately after enucleation and 58 from 24 eyes undergoing intravitreal injection of chemotherapy. No eyes were excluded from evaluation. Five of the 63 AH samples (8%) were removed due to poor read count alignment (<2%). Of the remaining 58 samples, 40 exhibited any SCNA above threshold (69%) and 34 (57%) demonstrated one or more of the highly recurrent `RB SCNAs,' namely, gains of 1q, 2p, 6p, focal *MYCN* amplification and losses at 13q and 16q (refs. 9, 10, 13, 40; Table 1). The focus of this analysis is on these RB SCNAs; however, alterations in other chromosomal segments were included when scoring total genomic instability (Supplementary Figs. S1 and S2). In agreement with prior analyses of retinoblastoma tumors (9), the overall genomic instability in the AH samples, defined as the total sum deviation from the median of the genome with CNAs, positively correlated with age at diagnosis ($P = <0.0001$, $R^2 = 0.658$). This observation lends further credence to the hypothesis that the AH is a valid and reliable source of tumor-derived DNA for retinoblastoma (Supplementary Fig. S1).

Genomic analysis of the AH demonstrates similar profiles to matched tumors

We sought to assess whether cfDNA in the AH sample resembles that of the tumor cells when the same eye is subsequently enucleated (Fig. 2). Concordance of DNA profiles between tumor and the initial AH sample ranged from 84.3% to 100%. Eleven of the 13 eyes showed a near-exact match of chromosomal gains and losses between tumor and AH (>90% concordance). Case 1 was similar (84.3% concordance), but the CNAs in the AH did not exactly mimic the tumor. This patient had germline loss of a 13q segment predisposing to development of retinoblastoma. This eye (previously described; ref. 21) had multiple retinal tumors at diagnosis that had likely developed different subsets of SCNAs. Case 4 (85.1% concordance) is a patient without a germline *RB1* mutation but similarly developed multiple recurrent subretinal tumors from reactivated seeding poorly responsive to therapy and was subsequently enucleated. We hypothesize that in these cases, the AH cfDNA profile was a heterogeneous mixture of tumor-derived DNA from each tumor clone. We observed that the genomic status of the AH matches the genomic status of the tumor, except when multiple retinal tumors were present.

Genomic analysis of AH samples longitudinally demonstrates reproducibility

We next evaluated the genomic status of the tumor at multiple time points corresponding to sequential intravitreal injections. To determine whether AH SCNA profiles were stable over time, and correlate with matched tumors, we compared AH and tumor profiles using two different methods. We evaluated the intersample concordance for 58 samples from 21 eyes that had more than 1 sample of AH and/or matched tumor available. Figure 3 shows a hierarchical clustering matrix (Pearson) containing AH and tumor samples from this subset of samples. Using this method, we observed that tumor samples

Table 1. Patient demographics, clinical outcomes, and RB SCNA genomic alterations

Case	Sex	Age at Dx (mos)	IIRC group class	TNM	Laterality	Seed class	Blood *RB1* mutation	Initial Tx	Req'd laser &/or Cryo	# Laser sessions	# Cryo sessions	Req'd IVM	Timing of 1st AH sample	Total # of AH samples	Conc. DNA ng/μL	 1q	 2p	 6p	 13q	 16q	Any RB SCNA	Req'd ENUC?	Reason for ENUC	High-risk path?	Time to ENUC after dx (days)	Follow-up (mos)
1	M	20	E	cT3c	U	Cloud	13q^{-}	ENUC	NA	NA	NA	NA	With enuc	1	31.1			↑(2.0)	↓(0.5)		Yes	Yes	Primary	Yes	0	19
2	M	7	E	cT3b	U	Cloud	Negative	ENUC	NA	NA	NA	NA	With enuc	1	56			↑(2.6)			Yes	Yes	Primary	No	14	8
3	M	38	E	cT2b	U	Dust	Negative	ENUC	NA	NA	NA	NA	With enuc	1		↑(1.3)		↑(1.5)		↓(0.5)	Yes	Yes	Primary	Yes	2	8
4	M	26	D	cT2b	U	Sphere	Negative	CEV	Yes	6	4	Yes	IVM	2	0.23^{++}	↑(1.4)	↑(1.8)			↓(0.6)	Yes	Yes	Recur	No	511	17
5	M	0	B	cT1b	B	Dust***	g.76932_76952del21	CEV	Yes	22	1	Yes	IVM	1	0.18						No**	Yes	Recur	Yes	1,166	49
6	F	28	D	cT2b	B	Cloud	30% mosaic c.1075>T	CEV	Yes	15	2	Yes	IVM	7	0.14^{++}	↑(1.5)	↑(1.3)	↑(2.0)		↓(0.6)	Yes	Yes	Recur	No	537	37
7	M	10	E	cT3c	B	Dust	Frameshift mtn exon 18	CEV	Yes	12	0	Yes	IVM	1				↑(1.6)			Yes	Yes	Recur	Yes	13	38
8	F	22	D	cT2b	U	Dust	Negative	CEV	Yes	10	0	Yes	IVM	3		↑(1.1)		↑(1.7)		↓(0.7)	Yes	Yes	Recur	No	257	9
9	F	29	D	cT2b	B	Sphere	c.958C>T Exon 10	CEV	Yes	6	0	No	With enuc	1		↑(1.7)		↑(1.5)			Yes	Yes	Persist	No	246	22
10	F	2	E	cT3c	B	Dust	c.2425delC	CEV	No	0	0	No	With enuc	1			Focal ***MYCN***				yes	yes	Persist	No	86	18
11	F	8	D	cT2b	U	Dust	Negative	CEV	Yes	15	5	Yes	IVM	4				↑$^{+}$(1.5)			Yes	Yes	Recur	No	426	14
12_OS	F	13	D	cT2b	B	Sphere	13q and 16 p deletion	CEV	Yes	7	3	Yes	IVM	1				↑(1.8)	↓(0.5)		Yes	Yes	Recur	No	300	13
13	M	34	D	cT2b	U	Sphere	p.Met148Valf	CEV	Yes	8	1	Yes	IVM	2		↑(1.2)		↑(1.5)		↓(0.7)	Yes	Yes	Recur	No	302	11
12_OD	F	13	C	cT2b	B	Dust	13q and 16 p deletion	CEV	Yes	4	0	Yes	IVM	3		↑(1.3)			↓(0.5)	↓(0.7)	Yes	No	NA	NA	NA	13
14	M	5	D	cT2b	U	Sphere	Negative	CEV	Yes	20	3	Yes	IVM	1	0.88^{++}						No	No	NA	NA	NA	26
15	M	10	D	cT2b	U	Dust	Negative	IAM	Yes	13	0	Yes	IVM	3							No	No	NA	NA	NA	16
16_OD	M	9	E	cT3b	B	Dust	c.2527delG (Exon 25)	CEV	Yes	15	0	Yes	IVM	2							No	No	NA	NA	NA	16
16_OS	M	9	E	cT3b	B	Dust	c.2527delG (Exon 25)	CEV	Yes	15	0	Yes	IVM	3							No	No	NA	NA	NA	16
17	F	2	E	cT3c	B	Sphere	c.1421+12_1421+32del21bp	CEV	Yes	19	0	Yes	IVM	2							No	No	NA	NA	NA	23
18_OD	M	26	C	cT2b	B	Dust	c.2520+1G>A (intron 24)	CEV	Yes	7	1	Yes	IVM	1		↑(2.0)		↑(1.7)		↓(0.5)	Yes	No	NA	NA	NA	19
18_OS	M	26	D	cT2b	B	Cloud	c.2520+1G>A (intron 24)	CEV	Yes	6	0	Yes	IVM	1				↑(1.5)		↓(0.5)	Yes	No	NA	NA	NA	19
19	F	26	D	cT2b	B	Dust	c.1981C>T (exon 20)	IAM	Yes	10	0	Yes	IVM	3							No	No	NA	NA	NA	25
20	F	2	D	cT2b	B	Sphere	T→G in exon 17	CEV	Yes	6	0	Yes	IVM	3							No	No	NA	NA	NA	30
21	M	24	D	cT2b	B	Dust	Negative	CEV	Yes	2	0	Yes	IVM	2		↑(1.4)		↑*(1.2)	↓(0.1)	↓(0.5)	Yes	No	NA	NA	NA	25
22	M	28	D	cT2b	U	Cloud	c.1981C>T (exon 20)	CEV	Yes	3	1	Yes	IVM	5		↑(1.5)	↑(1.3)			↓(0.5)	Yes	No	NA	NA	NA	26
23	M	4	D	cT2b	U	Dust	Negative	CEV	Yes	5	0	Yes	IVM	1							No	No	NA	NA	NA	35
24	F	10	D	cT2b	U	Dust	Negative	CEV	Yes	13	0	Yes	IVM	3	0.29^{++}						No	No	NA	NA	NA	42
25	F	59	D	cT2b	U	Dust	Negative	CEV	Yes	12	6	Yes	IVM	2	0.30^{++}			↑*(1.2)	↓(0.6)		Yes	No	NA	NA	NA	42
26	M	2	D	cT2b	U	Dust	Negative	CEV	Yes	15	1	Yes	IVM	2							No	No	NA	NA	NA	17

NOTE: Eyes that required enucleation are above the gray line and those that were salvaged are below. Gains or losses are indicated as ↑ gain; ↓ loss, along with amplitude of the change (as ratio to median).
Abbreviations: AH, aqueous humor; CEV, carboplatin; ENUC, enucleation; mos, months; mtn, mutation; RB, retinoblastoma; *RB1*, retinoblastoma tumor suppressor gene; SCNA, somatic CNA; Tx, therapy.
$^{+}$SCNA not present in the initial AH sample, but present in subsequent (case 11).
*SCNA present in the initial AH sample but NOT present in subsequent (cases 21 and 25).
**SCNA not present in initial AH sample however required secondary enucleation for a late (>800 days) massive retinal recurrence and AH was not taken at that time (case 5).
$^{++}$Median value based on multiple samples evaluated.
***Seeds not present at diagnosis, present with recurrence only.

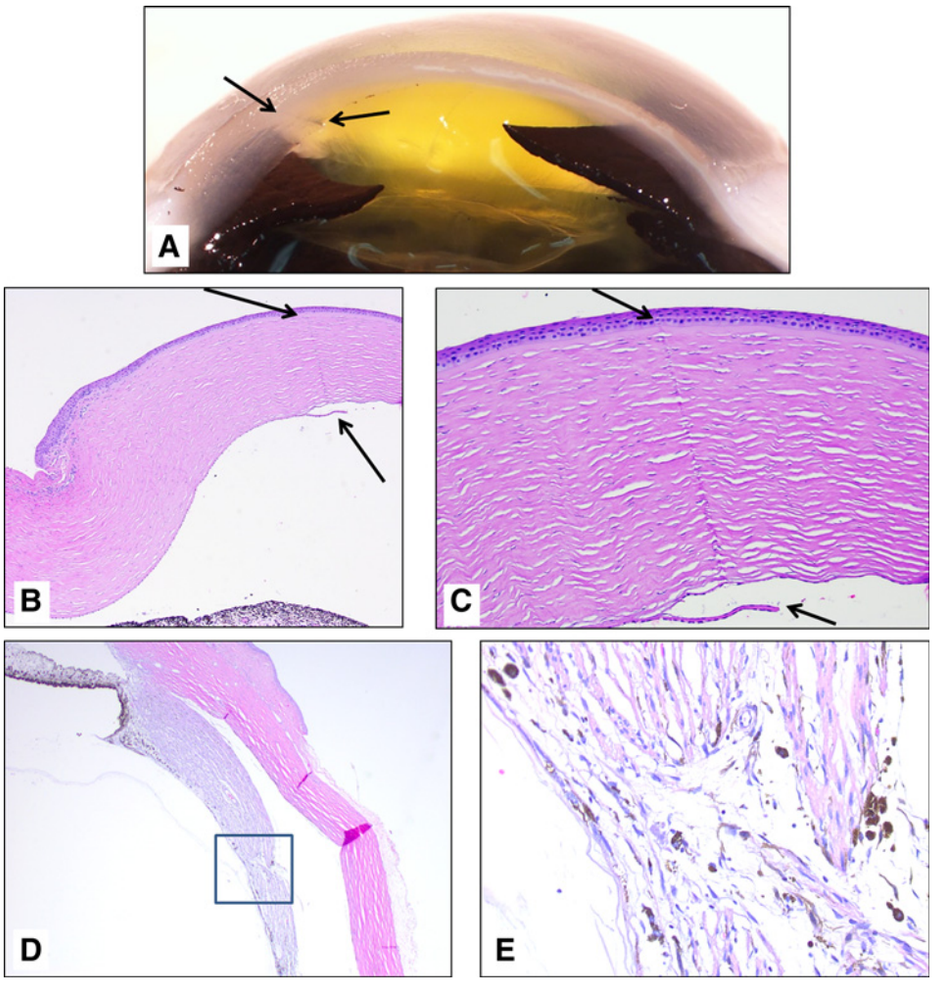

Figure 1.
Histopathology from an eye enucleated after intravitreal injection. **A,** Paracentesis site in the cornea on gross examination (**B**) at 40× and (**C**) 100×. No tumor was seen in the needle tracks from the paracentesis in the cornea. The cornea tracks were well healed and without tumor. **D,** The pars plana entrance of the injection site for intravitreal melphalan at 40× and (**E**) at 100× also showed healed tissue without evidence of tumor cells.

correlate most closely with matched AH samples from the same eye (with the exception of case 1, described above). The majority of longitudinal AH samples also group together with few exceptions. For example, in case 15, AH samples 1 and 2 clustered together but sample 3, taken at the last intravitreal injection, had reduced amplitude of alterations and clustered instead with those samples with fewer, lower amplitude aberrations. This demonstrates the high level of intersample concordance in the AH with genomic alterations (including low amplitude alterations) remaining stable over sequential draws. The same information for all AH samples arranged in genome order is shown in Supplementary Fig. S2.

SCNA profiling of AH cfDNA reveals differences in enucleated and salvaged eyes

Another goal of this study was to determine whether genomic evaluation of the AH was predictive of eye salvage. We directly compared the initial AH cfDNA CNA profiles for eyes that had been enucleated versus salvaged (Fig. 4; Supplementary Figs. S3 and S4). Genomic evaluation of these AH samples demonstrated the presence of any RB SCNA in enucleated eyes was 12/13 (92%), whereas the fraction in salvaged eyes was 6/16 (38%; $P = 0.006$). Of the RB SCNAs, 6p gains were the most frequent RB SCNA and were significantly more common in enucleated eyes. The 6p gain was present in 10/13 enucleated eyes (77%) as compared with 4/16 (25%) salvaged eyes (Fisher exact, $P = 0.0092$). The composite summation of the SCNA profiles from the initial AH samples for the two groups is shown in Fig. 4 revealing the difference in median (of the ratio to the median) amplitude of 6p gain between enucleated and salvaged eyes (1.47 in enucleated eyes vs. 1.07 in salvaged eyes, $P = 0.001$). There were no significant differences in 1q, 2p, 13q, or 16q between the salvaged and enucleated groups, although there was a marginal effect for 1q (1.22 median amplitude gain in enucleated eyes, vs. 1.09 gain in salvaged eyes, $P = 0.08$). We noted a focal *MYCN* amplification on 2p without any other SCNAs in the AH of one eye (case 10; Supplementary Fig. S3). The odds of an eye requiring enucleation were 20-fold greater if any RB SCNA was present in the AH (OR, 20.0; 95% CI,2.1–195.0, logistic regression); and 10-fold greater if 6p gain was present in the AH (OR, 10.0; 95% CI, 1.8–55.6, logistic regression).

In order to evaluate the independent effects of each candidate biomarker on ocular salvage, while accounting for age and any predictive utility of staging information, we created a multivariable Cox proportional hazard model. Based on univariable Kaplan–Meier analyses, we reduced staging to two levels (D or E vs. A, B, or C) and collapsed all other SCNA deviations than 6p gain to another dichotomous variable. Using this model, the risk

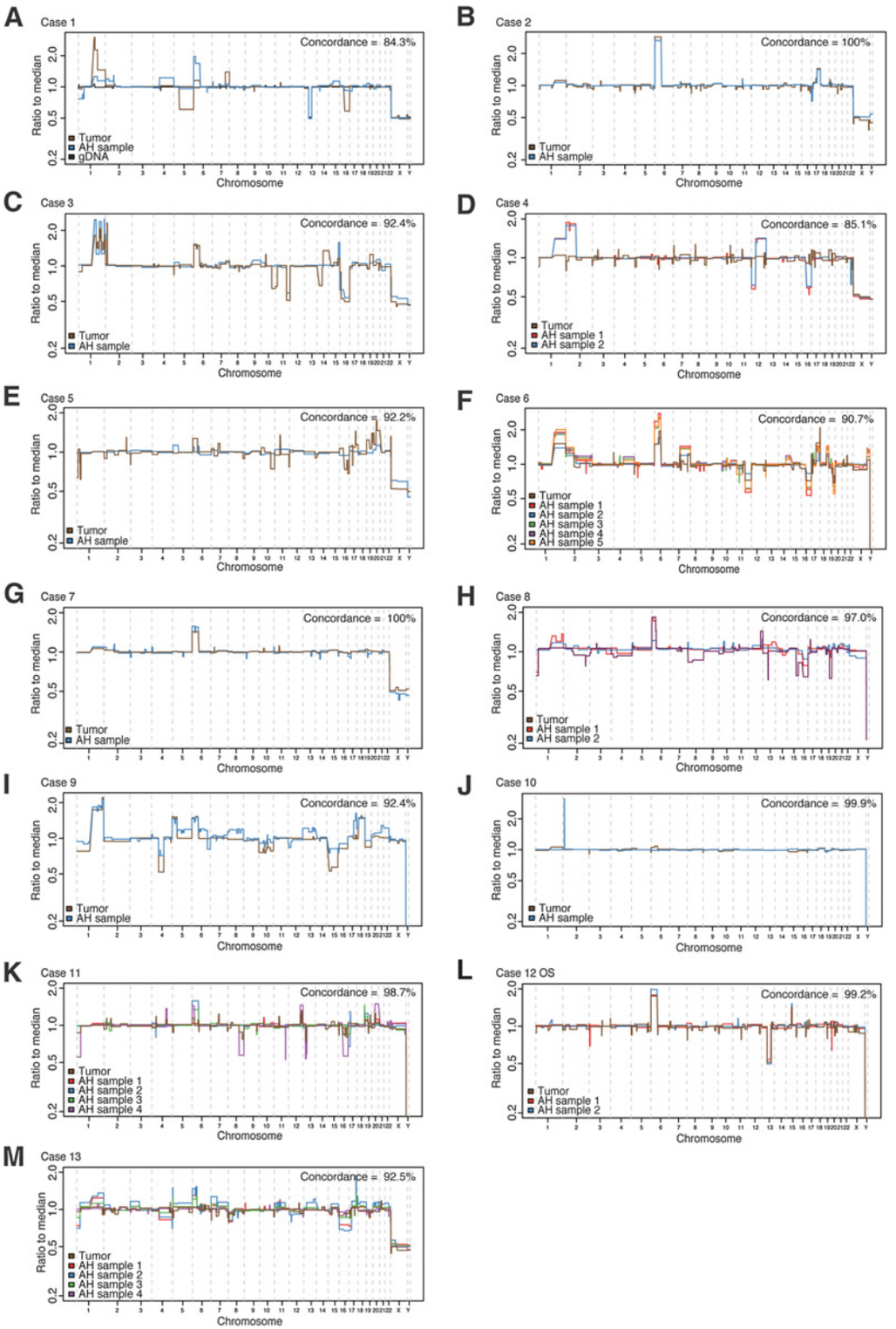

Figure 2.

Chromosomal CNA profiles from 13 eyes that required enucleation with available tumor tissue for comparison. The profiles demonstrate the similar genomic alterations: concordance of DNA profiles between tumor and the iAH ranged from 84.3–100%. Eleven of the 13 eyes showed a near exact match of chromosomal gains and losses between tumor and AH (>90% concordance).

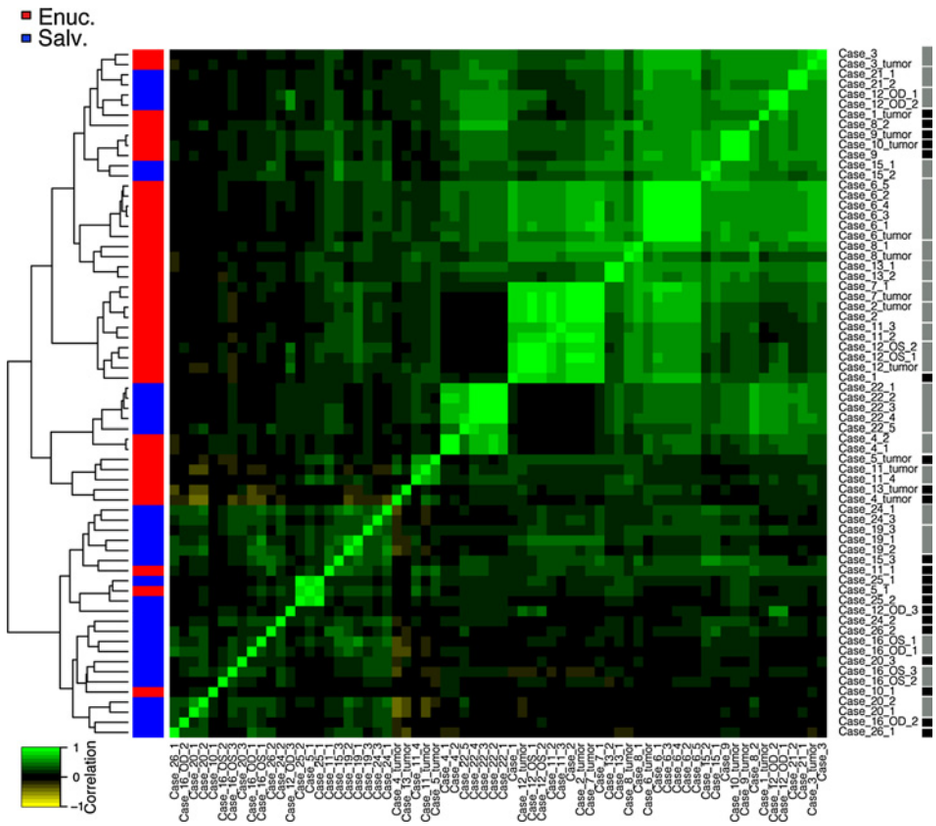

Figure 3.
Pearson hierarchical clustering matrix based on the SCNA profiles of the 58 AH and tumor samples from 21 eyes that had more than one sample available for correlation. Samples are listed as case number_# based on the chronological order of AH sampling (e.g., 1, 2, 3). Tumor samples correlate most closely with the matched AH samples from the same eye (with the notable exception of case 1, described in the text). The majority of longitudinal AH samples also group together with few exceptions. Samples that correlate within the same eye are shown by the gray bars on the right; the black bars indicate samples that did not fall adjacent other samples from the same eye. Samples from eyes that were enucleated (e.g., surgically removed) are indicated by the red bar adjacent the dendogram, those that are salvaged (e.g., saved) are indicated in blue.

of enucleation was 2.14 times greater in patients with 6p gain (Bootstrapped HR, 2.14; 95% CI, 1.29–3.58; $P = 0.01$) and 1.17 times greater for patients who carried any other SCNA (Bootstrapped HR, 1.17; 95% CI, 0.57–2.40; $P > 0.05$), although the latter was not statistically significant in the multivariable model. Notably, the interaction between age and analysis time was not significant, verifying the proportional hazard assumption.

The presence of RB SCNAs, specifically gain of 6p, in the AH improves upon clinical classification alone for prediction of eye salvage

It is known that clinical classification [IIRC, ref. 3; tumor–node–metastasis (TNM), ref. 8] predicts eye salvage; however, prognostic success remains limited for advanced eyes (4–7, 23). Thus, to test whether genomic analysis of AH samples could better predict eye salvage, genomic instability, presence of RB SCNAs, and specifically 6p gain were analyzed in addition to clinical IIRC and TNM classification for ocular survival. Kaplan–Meier curves were evaluated at 1 standard deviation from the median follow-up (800 days). The primarily enucleated eyes (cases 1–3) were removed as salvage was not attempted.

We then evaluated ocular survival based on AH genomics. We first evaluated whether overall genomic instability was a useful biomarker for eye salvage with Cox proportional hazard modeling; this was not shown to be predictive ($P = 0.5882$; 95% CI, 0.9982–1.0025). We used 300 as a marker of "high" genomic instability which also did not predict ocular survival based on Kaplan–Meier analysis (Fig. 5A, log-rank, $P = 0.1373$). However, the presence of RB SCNAs in the AH predicted eye salvage significantly better than clinical classification alone (Fig. 5B, $P = 0.0028$). Within the RB SCNAs, gain of 6p was the single SCNA that was most predictive of inability to salvage the eye (Fig. 5C, $P = 0.0092$). Only 4 eyes had other RB SCNAs and *not* gain of 6p; two were in the enucleated group (cases 4 and 10) and two in the salvaged group (cases 12 and 22).

Given that gain of 6p was the single most predictive SCNA, we then evaluated the impact of this objective genomic information in addition to clinical classification for both IIRC and TNM classification. Figure 5D shows that IIRC classification alone does stratify eye survival by class, demonstrating that advanced D and E eyes have a lower likelihood of eye salvage, although in this small group this was not significant ($P = 0.6716$). This is similar when TNM classification is used (Fig. 5G, $P = 0.2400$).

Evaluation of both clinical and genomic information (e.g., gain of 6p) in advanced group D and E eyes also demonstrates that genomic analyses increased the predictive value of tumor relapse requiring enucleation (Fig. 5E, $P = 0.0130$; Fig. 5F, $P = 0.2207$). This was similarly seen for advanced cT2b and cT3 eyes with the TNM classification (Fig. 5H; $P = 0.0174$; Fig. 5I, $P = 0.2207$). It should be noted that the 5 group E eyes are the same 5 cT3 eyes as the clinical classification schemes are similar.

Longitudinal evaluation of AH samples may predict tumor remission and relapse

Despite the relative genomic stability of the AH samples (Fig. 3), we observed measurable differences in the amplitude of these alterations over the course of treatment in a manner that correlated with clinical response to therapy. We interpret the changes in amplitude to reflect the fraction of tumor DNA in the total AH cfDNA and by inference, tumor activity.

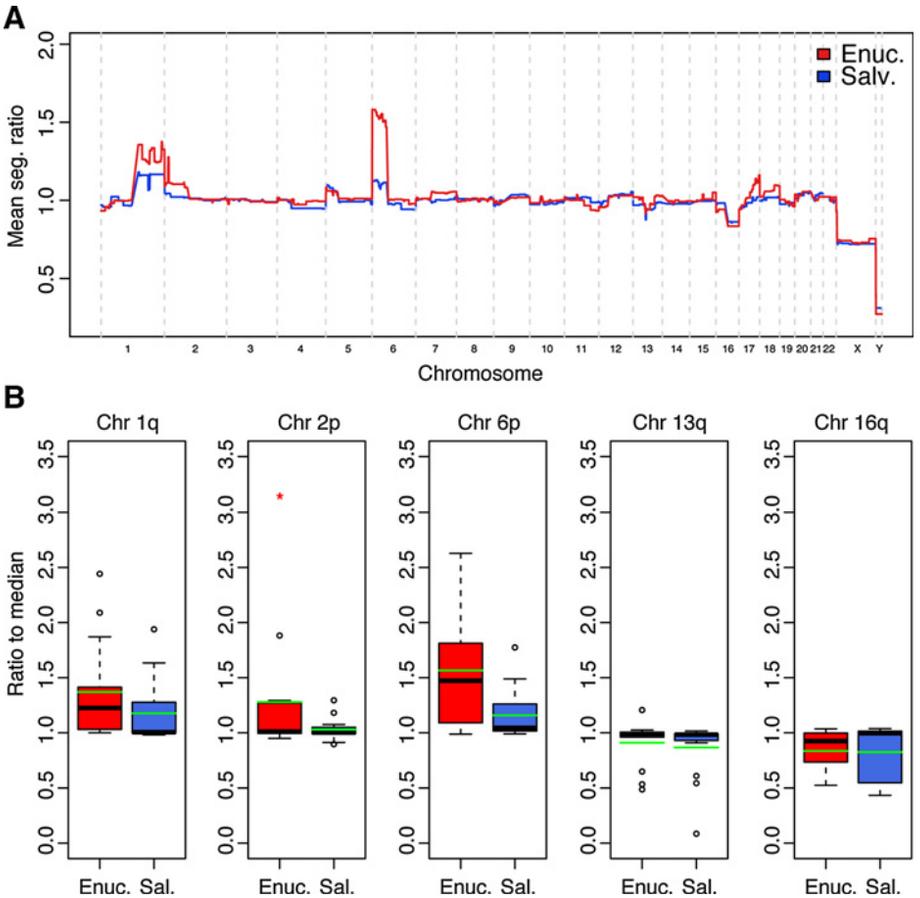

Figure 4.

A, Composite somatic CNA profile from cell-free DNA in the AH samples from enucleated eyes (Enuc, red) and salvaged eyes (Salv, blue). **B,** Box plot demonstrating the range of amplitude changes for the enucleated (Enuc) vs. salvaged (Salv) eyes; the black bar represents the median while the green bar represents the mean (of the ratio to median). The sample with focal *MYCN* gain is shown as a red asterisk in the Chr 2p plot. The median of the ratio to median amplitude of Chr 6p gain is significantly greater in enucleated eyes ($P = 0.001$), which may be both from the increased copy number of the amplified region and an increase in the total fraction of tumor-derived DNA in the AH of enucleated eyes.

Two patients in this cohort had >4 samples of AH available for evaluation. Case 22 had 5 AH samples taken during intravitreal injection of chemotherapy in which the seeds were treated successfully, the main retinal tumor did not recur, and this eye was successfully salvaged. Comparison of the AH profiles over time showed a decreasing burden of tumor-derived DNA in the AH with no additional chromosomal alterations appearing. In fact, a decrease in the amplitude of alterations below threshold was seen in the last sample. This suggests a gradual reduction in the fraction of tumor-derived DNA in the cfDNA extracted from the AH as the tumor responds to therapy (Fig. 6).

In contrast, case 6 (previously described; ref. 21) had 7 AH samples, of which 5 had acceptable read alignment. Evaluation of the AH SCNA profiles demonstrated an initial decrease in the amplitude of alterations indicating a reduced amount of tumor DNA in the AH and a positive response to the intravitreal chemotherapy. However, the subsequent AH samples show increased amplitude, correlating clinically with tumor recurrence; this eye required enucleation. The AH sample at the time of enucleation demonstrated an increased number of genomic events and instability (Fig. 6).

Amplitude changes specifically in 6p also correlated with clinical outcomes. Two eyes in the salvaged group had small amplitude gain in 6p in the first AH sample only, becoming greatly diminished or undetectable in later samples (cases 21 and 25). Similarly, one eye (case 11) that required enucleation did not initially have a gain of 6p. However, with tumor relapse, 6p gain was present in subsequent AH samples (Supplementary Fig. S5).

Taken together, these results indicate that increase or decrease in SCNA amplitude or total genomic instability could be useful as a real-time predictor of tumor response during treatment in certain cases.

Discussion

Herein, we present a novel analysis of retinoblastoma tumor DNA in 63 separate AH samples, the majority of which were taken during active treatment. Evaluation of this larger data set provided further evidence that the AH "surrogate tumor biopsy" (21) is a valid source of tumor-derived cfDNA and is representative of the genomic state of the tumor. With access to tumor DNA *in vivo*, we were able to identify differences in the SCNA profiles from enucleated and salvaged eyes. The differences in these genomic profiles significantly affected the prediction of therapeutic tumor response, retrospectively. Notably, we found that lack of a 6p gain confers a significant survival benefit for the eye ($P = 0.0092$); stated conversely, the presence of 6p gain in the AH was associated with a significantly increased risk of an eye requiring enucleation. Based on multivariate analysis, this risk is 2.14-fold greater; however, univariate analysis predicts a 10-fold greater risk of enucleation in an eye with 6p gain in the AH. Gain of 6p provided additional objective information beyond established clinical classifications to predict the likelihood of globe salvage for patients with advanced retinoblastoma. In addition to this objective measure, we found a potential benefit of longitudinal

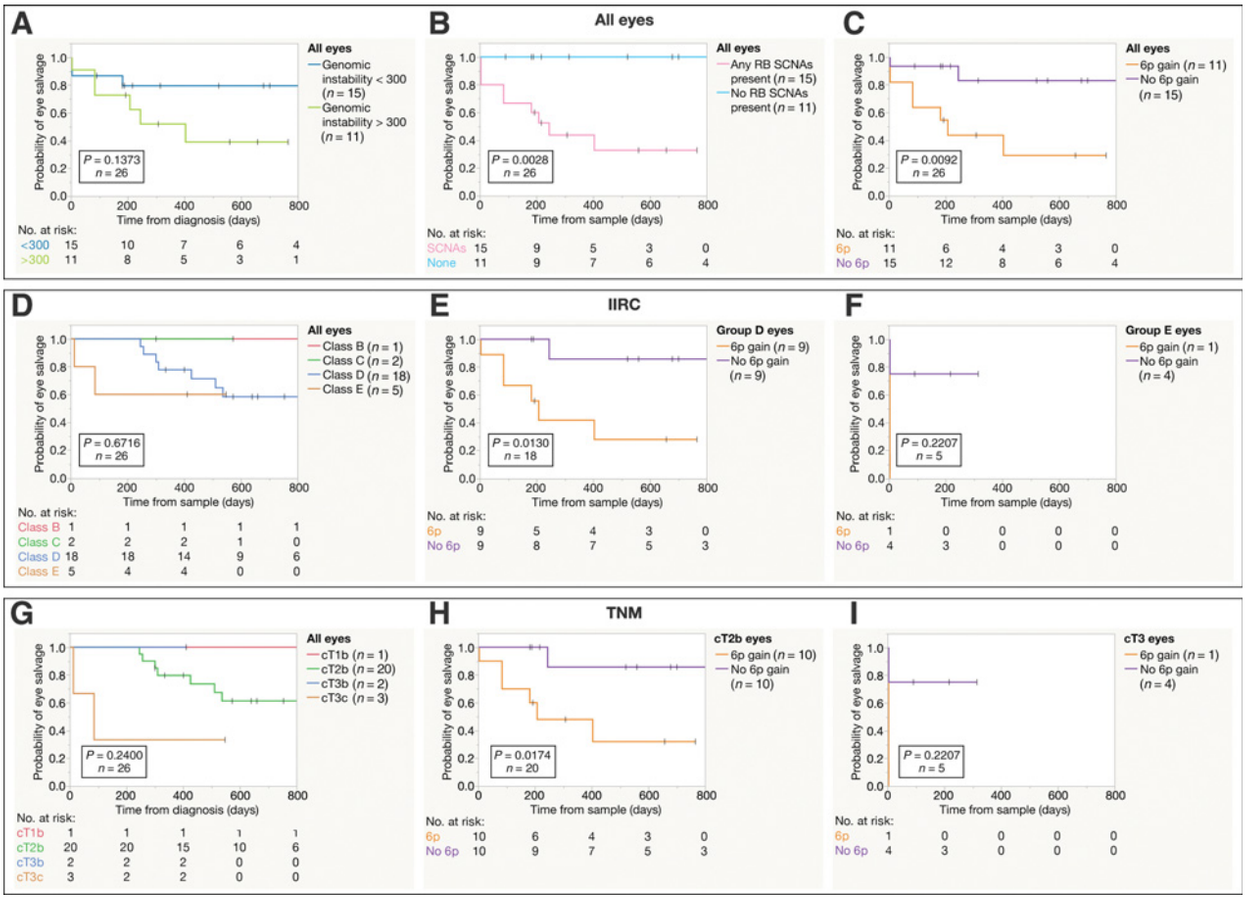

Figure 5.

Kaplan–Meier curves of eye salvage for treated eyes (e.g., no primary enucleations) at 800 days by ALL EYES: **A,** All eyes ± presence of genomic instability >300 sum deviation from the median (with time from sample to event or last follow-up), regardless of clinical classification; **B,** all eyes ± the presence of RB SCNAs in the AH (with time from sample to event or last follow-up), regardless of clinical classification; **C,** all eyes ± presence of gain of 6p in the AH (with time from sample to event or last follow-up), regardless of clinical classification; WITHIN IIRC; **D,** IIRC group (with time from diagnosis to event or last follow-up); **E,** Group D eyes ± gain of 6p in the AH (with time from sample to event or last follow-up); **F,** Group E eyes ± gain of 6p in the AH (with time from sample to event or last follow-up); WITHIN TNM. **G,** TNM group (with time from diagnosis to event or last follow-up). **H,** cT2b eyes ± gain of 6p in the AH (with time from sample to event or last follow-up). **I,** cT3 eyes ± gain of 6p in the AH (with time from sample to event or last follow-up). This demonstrates that the presence of any RB SCNA aids in prediction of globe salvage more accurately than group classification alone. Within the RB SCNAs, 6p gain was most predictive of risk of tumor recurrence requiring enucleation.

sampling of the AH as the overall amplitude of genomic alterations may provide a real-time measure of therapeutic response.

Although the analysis in this larger sample set provided further support for the clinical utility of the AH, it should be noted that cfDNA taken from a cancer patient, whether from blood or AH, is a variable mixture of normal DNA and DNA shed from the tumor. Thus, measurements of copy-number and peak amplitude of alterations reflect both the intrinsic genomic state of the tumor and the overall quantity of tumor DNA in the fluid. These AH samples were not taken at diagnosis, but rather after initial chemotherapy at the time of adjuvant IVM, or at the time of a tumor recurrence that required secondary enucleation. We retrospectively observed that enucleated eyes had a higher frequency of RB SCNAs, with greater amplitude of alterations, than salvaged eyes (Supplementary Figs. S1 and S2). Thus, the AH SCNA profiles with minimal alterations that were seen in the salvaged eyes may reflect a tumor with similarly few CNAs, or rather the response of the tumor to previous chemotherapy and thus a low fraction of tumor-derived cfDNA in the AH, or both. Additionally, the majority of included eyes were advanced group D and E; it is not clear if eyes with smaller tumor burden and/or less seeding would actively shed tumor DNA into the AH. At this point, we only know that following the treatment protocol at our institution, the AH profiles without the presence of RB SCNAs strongly correlated with therapeutic tumor response and the ability to save the eye. This may represent a minimally invasive means of detecting the risk of secondary enucleation at the time of a retinal or seeding recurrence. Without prospective studies, this cannot be extrapolated to predictions of therapeutic response at diagnosis and gain of 6p may or may not have a similar relationship to eye salvage with different treatment paradigms.

Of the RB SCNAs, 6p gain was the most frequently identified SCNA in the AH. Gains of 6p are also the most common genomic

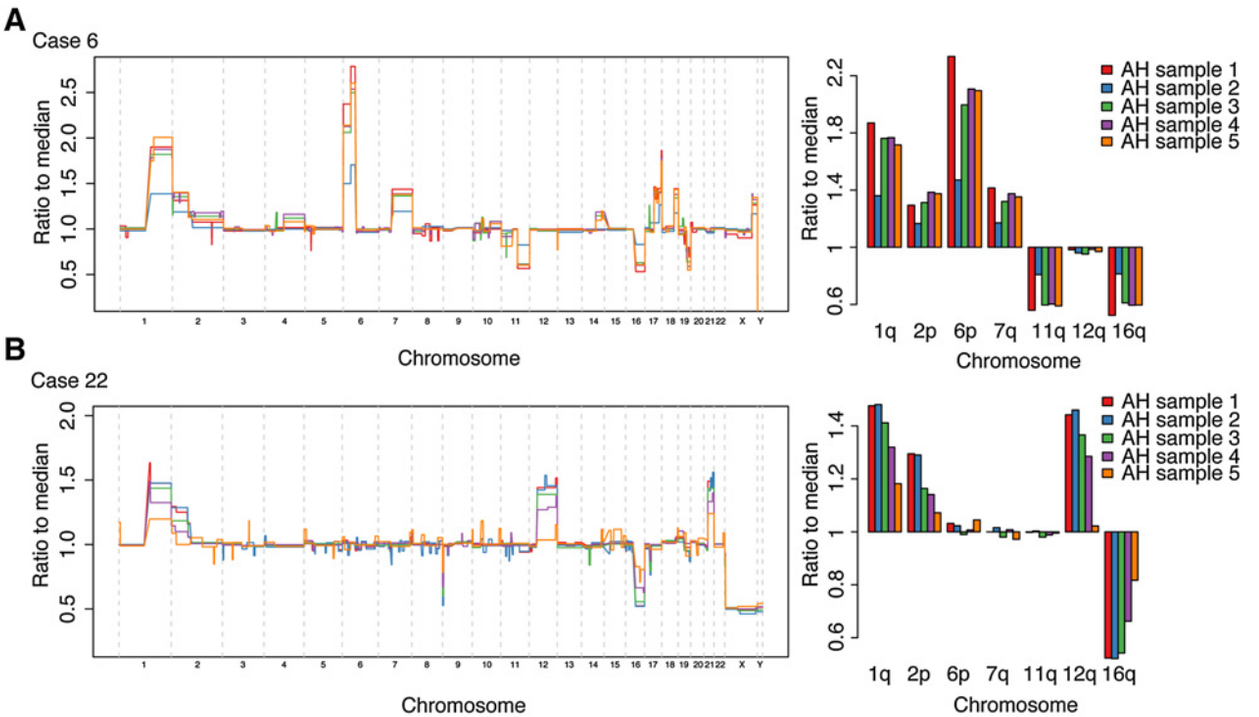

Figure 6.

CNA profile and histogram from two cases demonstrating changes in amplitude of alterations that correlate with clinical tumor response. The CNA profiles for case 6(**A**) demonstrates increased chromosomal alterations in chromosomes 1q, 2p, 6p, and 16q; additionally, 7q, 11q, and 12q were altered and are shown. AH samples 1 to 5 were taken longitudinally separated by at least 1 week between samples. Case 6 demonstrates decreased CNA magnitude at AH sample 2 relative to sample 1, which correlated with clinical response to therapy; however, these alterations then increase steadily with persistent tumor activity and this eye eventually required enucleation. The CNA profile from the tumor (shown in Fig. 2) mimics the AH profile. Case 22(**B**) demonstrates an opposite finding: as the tumor responded to therapy the CNA magnitude from the AH declined. This suggests both a smaller concentration of tumor-derived DNA as the tumor responds to therapy and a normalization of the chromosomal alterations.

changes observed in retinoblastoma tumors (14, 17). Driver genes for tumorigenesis associated with 6p gain have been postulated including *DEK* and *E2F3* (10, 14, 41). DEK encodes a DNA-binding protein that acts as an oncogene in multiple cancers (42, 43), and E2F3 is involved in transcriptional cell-cycle control, regulated by the retinoblastoma protein (pRB; ref. 44). A more exact delineation of the mechanism by which 6p gain promotes retinoblastoma progression has been hindered by the fact that focal SCNAs (those carrying only a few genes) are rare, with the exception of the 2p region encompassing *MYCN* (45). Thus, the minimum region of gain for 6p is not yet refined to the single gene level. Providing additional detail on the genetic mechanisms behind this RB SCNA is a potential benefit of the AH biopsy to increase the number and range of cases tested as the AH can be sampled from enucleated as well as salvaged eyes. This assay has the resolution to detect focal events as evidenced by the detection of narrow MYCN amplifications. Our preliminary retrospective evaluation of 6p gain as a biomarker in the AH demonstrated that this highly recurrent SCNA correlates with clinical outcomes in retinoblastoma eyes undergoing treatment. This has not previously been shown because tumor genomics have not previously been evaluated from salvaged eyes. We found that both the frequency and the amplitude of 6p gain were significantly higher in the cohort of eyes that required enucleation and had significant predictive value. With access to tumor-derived cfDNA via the AH, future studies may explore associations with other clinical features and outcomes including type of tumor relapse, seeding class, high-risk histopathologic features, and metastatic disease.

Use of a biopsy to predict therapeutic response (46), risk of metastatic disease (47–49), and survival (50) for other malignancies, even other intraocular malignancies, has dramatically affected the ability to provide precision medicine for patients with other types of cancers. Liquid biopsies based on circulating tumor cells and cfDNA in the blood or other fluids have been explored for other cancers as means to further prognosticate therapeutic outcomes without the need for invasive tissue biopsy (51–55). Further investigation of the AH as a liquid source of tumor-derived cfDNA may improve our understanding of which genes contribute to retinoblastoma tumorigenesis, which biomarkers portend more aggressive disease activity and, in the future, may alter our current paradigms of disease management for this pediatric cancer. Our findings suggest that a prospective study with AH sampled at diagnosis and throughout therapy is warranted to further elucidate the impact of 6p gain or other biomarkers for retinoblastoma.

Disclosure of Potential Conflicts of Interest

J.L. Berry has ownership interest in a provisional patent application filed, not yet awarded. A.L. Murphree has ownership interest (including stock, patents, etc.) in eye imaging system US 5608472 A. J.B. Hicks has ownership interest

(including stock, patents, etc.) in Epic Sciences Inc., is a consultant/advisory board member for Epic Sciences, Inc., and Celmatix, Inc. No potential conflicts of interest were disclosed by the other authors.

Authors' Contributions

Conception and design: J.L. Berry, L. Xu, A.L. Murphree, T.C. Lee, P. Kuhn, J. Hicks
Development of methodology: J.L. Berry, L. Xu, B.J. Reiser, J. Hicks
Acquisition of data (provided animals, acquired and managed patients, provided facilities, etc.): J.L. Berry, L. Xu, A.L. Murphree, K. Stachelek, L. Welter, B.J. Reiser
Analysis and interpretation of data (e.g., statistical analysis, biostatistics, computational analysis): J.L. Berry, L. Xu, I. Kooi, R.K. Prabakar, M. Reid, B.H.A. Le, T.C. Lee
Writing, review, and/or revision of the manuscript: J.L. Berry, L. Xu, I. Kooi, M. Reid, R. Jubran, T.C. Lee, J.W. Kim, P. Kuhn, D. Cobrinik, J. Hicks
Administrative, technical, or material support (i.e., reporting or organizing data, constructing databases): J.L. Berry, M. Reid, B.H.A. Le, B.J. Reiser
Study supervision: J.L. Berry, P. Kuhn, J. Hicks
Other (interpretation and analysis of retinoblastoma enucleated eyes, review of needle tracks for obtaining anterior chamber taps and tumor injections): P. Chévez-Barrios

Acknowledgments

This study was supported by the Knights Templar Eye Foundation, The Larry and Celia Moh Foundation, The Institute for Families, Inc., Children's Hospital Los Angeles, an unrestricted departmental grant from Research to Prevent Blindness, Vicky Joseph Research Fund, Carol Vassiliadis Research Fund, USC Dornsife College of Letters, Arts and Sciences, and NCI of the NIH Award Number K08CA232344.

The costs of publication of this article were defrayed in part by the payment of page charges. This article must therefore be hereby marked *advertisement* in accordance with 18 U.S.C. Section 1734 solely to indicate this fact.

Received April 14, 2018; revised June 28, 2018; accepted July 18, 2018; published first July 30, 2018.

References

1. Fabian ID, Stacey AW, Johnson KC, Chowdhury T, Duncan C, Reddy MA, et al. Primary enucleation for group D retinoblastoma in the era of systemic and targeted chemotherapy: the price of retaining an eye. Br J Ophthalmol 2018;102:265–71.
2. Mendoza PR, Grossniklaus HE. Therapeutic options for retinoblastoma. Cancer Control 2016;23:99–109.
3. Linn Murphree A. Intraocular retinoblastoma: the case for a new group classification. Ophthalmol Clin North Am 2005;18:41–53.
4. Shields CL, Mashayekhi A, Au AK, Czyz C, Leahey A, Meadows AT, et al. The international classification of retinoblastoma predicts chemoreduction success. Ophthalmology 2006;113:2276–80.
5. Berry JL, Jubran R, Kim JW, Wong K, Bababeygy SR, Almarzouki H, et al. Long-term outcomes of Group D eyes in bilateral retinoblastoma patients treated with chemoreduction and low-dose IMRT salvage. Pediatr Blood Cancer 2013;60:688–93.
6. Kaliki S, Shields CL, Rojanaporn D, Al-Dahmash S, McLaughlin JP, Shields JA, et al. High-risk retinoblastoma based on international classification of retinoblastoma: analysis of 519 enucleated eyes. Ophthalmology 2013; 120:997–1003.
7. Shields CL, Manjandavida FP, Lally SE, Pieretti G, Arepalli SA, Caywood EH, et al. Intra-arterial chemotherapy for retinoblastoma in 70 eyes: outcomes based on the international classification of retinoblastoma. Ophthalmology 2014;121:1453–60.
8. Mallipatna A, Gallie BL, Chévez-Barrios P, Lumbroso-Le Rouic L, Chantada GL, Doz F, et al. AJCC Cancer Staging Manual Vol. 8th Edition. Amin SBE MB, Greene FL, editor: Springer; 2017.
9. Kooi IE, Mol BM, Massink MP, Ameziane N, Meijers-Heijboer H, Dommering CJ, et al. Somatic genomic alterations in retinoblastoma beyond RB1 are rare and limited to copy number changes. Sci Rep 2016;6:25264.
10. Kooi IE, Mol BM, Massink MP, de Jong MC, de Graaf P, van der Valk P, et al. A meta-analysis of retinoblastoma copy numbers refines the list of possible driver genes involved in tumor progression. PLoS One 2016; 11:e0153323.
11. Li WL, Buckley J, Sanchez-Lara PA, Maglinte DT, Viduetsky L, Tatarinova TV, et al. A rapid and sensitive next-generation sequencing method to detect RB1 mutations improves care for retinoblastoma patients and their families. J Mol Diagn 2016;18:480–93.
12. Rushlow DE, Mol BM, Kennett JY, Yee S, Pajovic S, Theriault BL, et al. Characterisation of retinoblastomas without RB1 mutations: genomic, gene expression, and clinical studies. Lancet Oncol 2013;14:327–34.
13. Theriault BL, Dimaras H, Gallie BL, Corson TW. The genomic landscape of retinoblastoma: a review. Clin Exp Ophthalmol 2014;42:33–52.
14. Corson TW, Gallie BL. One hit, two hits, three hits, more? Genomic changes in the development of retinoblastoma. Genes Chromosomes Cancer 2007;46:617–34.
15. Dimaras H, Khetan V, Halliday W, Orlic M, Prigoda NL, Piovesan B, et al. Loss of RB1 induces non-proliferative retinoma: increasing genomic instability correlates with progression to retinoblastoma. Hum Mol Genet 2008;17:1363–72.
16. Kapatai G, Brundler MA, Jenkinson H, Kearns P, Parulekar M, Peet AC, et al. Gene expression profiling identifies different sub-types of retinoblastoma. Br J Cancer 2013;109:512–25.
17. Cano J, Oliveros O, Yunis E. Phenotype variants, malignancy, and additional copies of 6p in retinoblastoma. Cancer Genet Cytogenet 1994;76:112–5.
18. Grasemann C, Gratias S, Stephan H, Schuler A, Schramm A, Klein-Hitpass L, et al. Gains and overexpression identify DEK and E2F3 as targets of chromosome 6p gains in retinoblastoma. Oncogene 2005;24: 6441–9.
19. Karcioglu ZA. Fine needle aspiration biopsy (FNAB) for retinoblastoma. Retina 2002;22:707–10.
20. Karcioglu ZA, Gordon RA, Karcioglu GL. Tumor seeding in ocular fine needle aspiration biopsy. Ophthalmology 1985;92:1763–7.
21. Berry JL, Xu L, Murphree AL, Krishnan S, Stachelek K, Zolfaghari E, et al. Potential of aqueous humor as a surrogate tumor biopsy for retinoblastoma. JAMA Ophthalmol 2017;135:1221–30.
22. Francis JH, Abramson DH, Ji X, Shields CL, Teixeira LF, Schefler AC, et al. Risk of extraocular extension in eyes with retinoblastoma receiving intravitreous chemotherapy. JAMA Ophthalmol 2017;135:1426–9.
23. Berry JL, Shah S, Bechtold M, Zolfaghari E, Jubran R, Kim JW. Long-term outcomes of Group D retinoblastoma eyes during the intravitreal melphalan era. Pediatr Blood Cancer 2017;64.
24. McShane LM, Altman DG, Sauerbrei W, Taube SE, Gion M, Clark GM, et al. Reporting recommendations for tumor marker prognostic studies (REMARK). J Natl Cancer Inst 2005;97:1180–4.
25. Munier FL, Soliman S, Moulin AP, Gaillard MC, Balmer A, Beck-Popovic M. Profiling safety of intravitreal injections for retinoblastoma using an anti-reflux procedure and sterilisation of the needle track. Br J Ophthalmol 2012;96:1084–7.
26. Baslan T, Kendall J, Rodgers L, Cox H, Riggs M, Stepansky A, et al. Genome-wide copy number analysis of single cells. Nat Protoc 2012;7:1024–41.
27. Baslan T, Kendall J, Rodgers L, Cox H, Riggs M, Stepansky A, et al. Corrigendum: Genome-wide copy number analysis of single cells. Nat Protoc 2016;11:616.
28. 2017 UCSC Genome Browser. Available from: https://genome.ucsc.edu/.
29. Langmead B, Salzberg SL. Fast gapped-read alignment with Bowtie 2. Nat Methods 2012;9:357–9.
30. Langmead B, Trapnell C, Pop M, Salzberg SL. Ultrafast and memory-efficient alignment of short DNA sequences to the human genome. Genome Biol 2009;10:R25.
31. Li H. A statistical framework for SNP calling, mutation discovery, association mapping and population genetical parameter estimation from sequencing data. Bioinformatics 2011;27:2987–93.
32. Huber W, Carey VJ, Gentleman R, Anders S, Carlson M, Carvalho BS, et al. Orchestrating high-throughput genomic analysis with Bioconductor. Nat Methods 2015;12:115–21.

33. Varin T, Bureau R, Mueller C, Willett P. Clustering files of chemical structures using the Szekely-Rizzo generalization of Ward's method. J Mol Graph Model 2009;28:187–95.
34. Strauss T, von Maltitz MJ. Generalising Ward's method for use with Manhattan distances. PLoS One 2017;12:e0168288.
35. Martelotto LG, Baslan T, Kendall J, Geyer FC, Burke KA, Spraggon L, et al. Whole-genome single-cell copy number profiling from formalin-fixed paraffin-embedded samples. Nat Med 2017;23: 376–85.
36. Berry JL, Bechtold M, Shah S, Zolfaghari E, Reid M, Jubran R, et al. Not all seeds are created equal: seed classification is predictive of outcomes in retinoblastoma. Ophthalmology 2017;124:1817–25.
37. Munier FL, Gaillard MC, Balmer A, Beck-Popovic M. Intravitreal chemotherapy for vitreous seeding in retinoblastoma: recent advances and perspectives. Saudi J Ophthalmol 2013;27:147–50.
38. Francis JH, Marr BP, Abramson DH. Classification of vitreous seeds in retinoblastoma: correlations with patient, tumor, and treatment characteristics. Ophthalmology 2016;123:1601–5.
39. Navin N, Hicks J. Future medical applications of single-cell sequencing in cancer. Genome Med 2011;3:31.
40. Kooi IE, Mol BM, Moll AC, van der Valk P, de Jong MC, de Graaf P, et al. Loss of photoreceptorness and gain of genomic alterations in retinoblastoma reveal tumor progression. EBioMedicine 2015;2: 660–70.
41. Bowles E, Corson TW, Bayani J, Squire JA, Wong N, Lai PB, et al. Profiling genomic copy number changes in retinoblastoma beyond loss of RB1. Genes Chromosomes Cancer 2007;46:118–29.
42. von Lindern M, Fornerod M, Soekarman N, van Baal S, Jaegle M, Hagemeijer A, et al. Translocation t(6;9) in acute non-lymphocytic leukaemia results in the formation of a DEK-CAN fusion gene. Baillieres Clin Haematol 1992;5:857–79.
43. Carro MS, Spiga FM, Quarto M, Di Ninni V, Volorio S, Alcalay M, et al. DEK expression is controlled by E2F and deregulated in diverse tumor types. Cell Cycle 2006;5:1202–7.
44. Adams MR, Sears R, Nuckolls F, Leone G, Nevins JR. Complex transcriptional regulatory mechanisms control expression of the E2F3 locus. Mol Cell Biol 2000;20:3633–9.
45. Mol BM, Massink MP, van der Hout AH, Dommering CJ, Zaman JM, Bosscha MI, et al. High resolution SNP array profiling identifies variability in retinoblastoma genome stability. Genes Chromosomes Cancer 2014;53:1–14.
46. Yun M, Bai HY, Zhang JX, Rong J, Weng HW, Zheng ZS, et al. ULK1: a promising biomarker in predicting poor prognosis and therapeutic response in human nasopharygeal carcinoma. PLoS One 2015;10:e0117375.
47. Onken MD, Worley LA, Ehlers JP, Harbour JW. Gene expression profiling in uveal melanoma reveals two molecular classes and predicts metastatic death. Cancer Res 2004;64:7205–9.
48. Onken MD, Worley LA, Tuscan MD, Harbour JW. An accurate, clinically feasible multi-gene expression assay for predicting metastasis in uveal melanoma. J Mol Diagn 2010;12:461–8.
49. Harbour JW. A prognostic test to predict the risk of metastasis in uveal melanoma based on a 15-gene expression profile. Methods Mol Biol 2014;1102:427–40.
50. Hicks J, Krasnitz A, Lakshmi B, Navin NE, Riggs M, Leibu E, et al. Novel patterns of genome rearrangement and their association with survival in breast cancer. Genome Res 2006;16:1465–79.
51. Tarazona N, Cervantes A. Liquid biopsy: another tool towards tailored therapy in colorectal cancer. Ann Oncol 2018;29:7–8.
52. Shukuya T, Patel S, Shane-Carson K, He K, Bertino EM, Shilo K, et al. Lung cancer patients with germline mutations detected by next generation sequencing and/or liquid biopsy. J Thorac Oncol 2018;13:e17–9.
53. Zhang W, Xia W, Lv Z, Ni C, Xin Y, Yang L. Liquid biopsy for cancer: circulating tumor cells, circulating free DNA or exosomes? Cell Physiol Biochem 2017;41:755–68.
54. von Bubnoff N. Liquid biopsy: approaches to dynamic genotyping in cancer. Oncol Res Treat 2017;40:409–16.
55. Baslan T, Kendall J, Ward B, Cox H, Leotta A, Rodgers L, et al. Optimizing sparse sequencing of single cells for highly multiplex copy number profiling. Genome Res 2015;25:714–24.